

# Split and Expand: An inference-time improvement for Weakly Supervised Cell Instance Segmentation

Lin Geng Foo<sup>1</sup>, Jiamei Sun<sup>1</sup>, and Alexander Binder<sup>2</sup>

<sup>1</sup> Singapore University of Technology and Design, Singapore

<sup>2</sup> University of Oslo, Norway

**Abstract.** We consider the problem of segmenting cell nuclei instances from Hematoxylin and Eosin (H&E) stains with dot annotations only. While most recent works focus on improving the segmentation quality, this is usually insufficient for instance segmentation of cell instances clustered together or with a small size. In this work, we propose a simple two-step post-processing procedure, Split and Expand, that directly improves the conversion of segmentation maps to instances. In the splitting step, we generate fine-grained cell instances from the segmentation map with the guidance of cell-center predictions. For the expansion step, we utilize Layer-wise Relevance Propagation (LRP) explanation results to add small cells that are not captured in the segmentation map. Although we additionally train an output head to predict cell-centers, the post-processing procedure itself is not explicitly trained and is executed at inference-time only. A feature re-weighting loss based on LRP is proposed to improve our method even further. We test our procedure on the MoNuSeg and TNBC datasets and show quantitatively and qualitatively that our proposed method improves object-level metrics substantially. Code for this paper will be made available after publication.

**Keywords:** Cell Instance Segmentation · Weakly Supervised · Computational Pathology

## 1 Introduction

Instance segmentation is a key step in many biomedical applications, such as phenotyping [6], cell-tracking [28] and computer-aided cancer diagnosis [10,5]. Deep learning models can potentially be used to master this task [13], leading to improvements in those applications, but require large amounts of high quality annotated data. Moreover, getting fully-annotated datasets of medical images is expensive. Using cloud annotation faces acceptance problems w.r.t. its reliability while it is time-consuming for qualified medical experts to annotate large databases. Conversely, it is much easier to obtain dot-annotated datasets, which is the primary motivating factor behind weakly-supervised segmentation.

The prevailing approach to tackle the weakly supervised segmentation problem consists of generating coarse labels using clustering and Voronoi partitioning, and training the segmentation model as usual using these labels [21,8,27,29].

While this approach works well for segmenting foreground pixels from the background, the conversion from the output segmentation map to the instance segmentation one is still coarsely done using basic morphological operations, leading to clumps of cells being identified as a single instance. Additionally, we also observe that small cells are often missed. This is potentially a big issue, especially when the number of cells detected is a primary concern, e.g cell counting.

In our work, we primarily focus on the instance segmentation problem. We modify the U-Net adapted from [7] by adding another head that does cell-center (CC) prediction in addition to the segmentation map, and simultaneously train both of these heads during training. During inference time, we post-process the segmentation map using our proposed two-step procedure: *Split* and *Expand*. In the *Split* step, we split up instances if they have multiple predicted cell-centers. In the *Expand* step, we expand the predicted CCs that were not identified in the segmentation map into cells. We use an explanation method, LRP, for this CC-Expansion task. LRP is capable of identifying the inputs that are related to the predictions and provides high-quality explanations and visualizations in many evaluation studies [20,23,3,17]. For the cell instances that are not captured in the segmentation maps but are shown in the CC predictions, we explain these CC predictions and identify those cells using the explanation results.

The CC-prediction task is challenging as the positive labels are sparse compared to the background. To get better accuracy on the CC output head, we propose a feature re-weighting (FRW) loss based on explanation methods inspired by [26]. Specifically, we construct an explanation-weighted feature for an intermediate layer of our segmentation model. The re-weighted features are then fed forward through the network to generate the FRW loss. With the FRW loss, the related features are refined further during gradient backpropagation and the CC-prediction performance is further improved. We test all our procedures on the MoNuSeg [16] and TNBC [18] datasets.

To summarize, our contributions are:

1. We propose a novel post-processing procedure, *Split and Expand*, for cell instance segmentation.
2. We employ cell center predictions to split segmented objects with multiple instances.
3. We explore using the explanations of cell center predictions to expand small cell instances. To our best knowledge, we are the first to segment cell instances with the guidance of explanation results.
4. We further propose a feature re-weighting loss to train the cell center output head, which leads to further improved object-level performance.
5. We remark that Split and Expand is training-free and model-agnostic. Experiments on MoNuSeg and TNBC datasets demonstrate the effectiveness of our proposed methods over the baseline.

## 2 Related Work

Several methods have been proposed to tackle the weakly-supervised cell segmentation problem. Notably, [21] pre-processed point labels into Voronoi cells and clusters based on color and used them as coarse labels. [30] proposed an edge network that could learn an edge map. [8] proposed a repel encoding loss that was applied in an alternating manner to the other losses. [19] posed a weakly-supervised domain adaptation problem and proposed an adversarial training method to tackle it. More recently, [22] proposed a weakly-supervised partial-annotations paradigm and self-supervised methods that perform well on that problem. [27] also proposed a self-supervised learning method together with a contour refinement technique. Throughout these works, the instance segmentation output is obtained by applying morphological operations on the output segmentation map. In this work, although we also apply the morphological operations to the segmentation maps, we also break up segments into smaller instances, as well as get new instances from expanding the cell-center prediction using explanation results obtained from LRP. We note that our work is distinct and complementary to the others proposed above, and can be easily added onto their methods.

In [11,9,29], a distance-map approach was applied to separate instances. Among them, only [29] considered the dot-annotated case, and is most closely related to our work. However, their approach is different from ours as they generate a new coarse label that approximates the distance labels and also requires training on those labels using the same architecture as [11].

LRP is one of the explanation methods that aim at de-mystifying the black box of deep neural networks (DNN) and interpreting the model decisions [4]. The explanations results reflect the contribution of a neuron to the model decision, which is helpful for understanding and debugging the models[17,1]. Recently, many works studied the use-cases of explanation results[12,26]. We also explore using LRP explanations to design a feature re-weighting loss for training and further improve the cell instance segmentation performance.

## 3 Method

### 3.1 Data pre-processing

Using the point labels, we generate three different types of coarse labels: Cluster, Voronoi, Enlarged Point. The Cluster and Voronoi labels are processed similar to [21]. Briefly speaking, the Cluster labels are a result of using K-Means on pixel values to get three clusters of pixels, which can then be assigned to be Cell, Background or Ambiguous classes. The Voronoi labels are obtained by applying Voronoi partitioning on the point labels. Lastly, the Enlarged Point labels are obtained by expanding each point label into a 3x3 square. This helps provide stronger supervision for the model. Other alternatives are possible, including expanding to a larger square, or applying a Gaussian function as in [19,22], but we find that simple 3x3 square labels suffice in training the CC outputs.

### 3.2 Cell-center predictions and feature re-weighting loss

A summary of our proposed network and losses can be seen in Figure 1. The U-Net generates features that will be used to generate the usual Segmentation output  $y_{seg}$  as well as an extra CC output  $y_{CC}$ . The Segmentation output is trained using pixel-wise cross-entropy loss with respect to the Cluster  $GT_C$  and Voronoi labels  $GT_V$ . The CC output is trained using pixel-wise cross entropy loss with respect to the Enlarged Point labels  $GT_P$ . Additionally, we also use a FRW loss  $L_{FRW}$  with respect to the Enlarged Point labels. The weights of the features are generated with the explanation results of LRP.

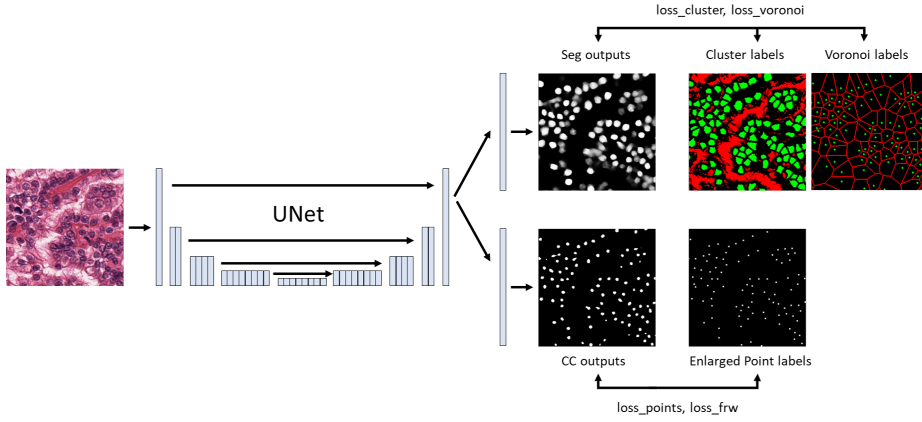


**Fig. 1.** An overview of our training method, network outputs, labels and losses.

LRP is capable of explaining various DNNs [4,2,24,14]. It assigns an explanation score to every neuron that reflects the supporting (positive scores) or opposing (negative scores) contribution to the predictions [17]. Furthermore, compared to other gradient-based explanation methods, LRP explanation scores reflect more of the related features that are used by the model to make decisions, which has been evaluated in [20,23,3]. Thus, we apply the LRP explanations to design the feature re-weighting loss,  $L_{FRW}$ . This loss has been known to perform well under the scenarios of small sample sizes or imbalanced datasets [26,25], and the latter case presents itself in our CC prediction task.

Let  $\mathbf{f}_l$  denote the feature map of layer  $l$  in our U-Net. We first perform a forward pass through the model to generate an original prediction  $y_{CC}$ . We then explain the generated prediction with LRP and obtain the explanation scores of the feature map  $R(\mathbf{f}_l)$ . We refer to the  $LRP_{\alpha 1}$  rule to calculate  $R(\mathbf{f}_l)$ , as suggested in [15]. The re-weighted feature  $\hat{\mathbf{f}}_l$  is calculated as follows:

$$w(\mathbf{f}_l) = l_{norm}(R(\mathbf{f}_l)) + 1, \hat{\mathbf{f}}_l = w(\mathbf{f}_l) \odot \mathbf{f}_l \quad (1)$$

where  $l_{norm}$  is a normalization layer where we divide using the maximum absolute value,  $w(\mathbf{f}_l)$  is the generated weight for feature map  $\mathbf{f}_l$ ,  $\odot$  is the Hadamard product operation, and  $\hat{\mathbf{f}}_l$  is the re-weighted feature. The re-weighted feature  $\hat{\mathbf{f}}_l$  is then fed forward to obtain a new output  $\hat{y}_{CC}$ , and the cross entropy loss is calculated with respect to the Enlarged Point labels.

With the re-weighting operation, we have  $w(\mathbf{f}_l) > 1$  for the features with positive LRP explanation scores (indicating support) and  $w(\mathbf{f}_l) < 1$  for those with negative LRP explanation scores (indicating opposition) [17,26]. Thus, the re-weighted features up-scale the related parts that are tuned more with  $L_{FRW}$ .

Our final losses for each output head is as follows, where  $\alpha_V, \alpha_C, \alpha_P, \alpha_{FRW}$  represent the weights of the Voronoi, Cluster, Point and FRW losses:

$$Loss_{seg} = L_V + L_C = \alpha_V CE(y_{seg}, GT_V) + \alpha_C CE(y_{seg}, GT_C) \quad (2)$$

$$Loss_{CC} = L_P + L_{FRW} = \alpha_P CE(y_{CC}, GT_P) + \alpha_{FRW} CE(\hat{y}_{CC}, GT_P) \quad (3)$$

### 3.3 Post-processing: Split and Expand

At test time, we obtain our Segmentation output and perform morphological operations (remove small objects, fill holes) to get an instance segmentation map. We then use our CC output to conduct a simple two-step post-processing (Instance-Splitting, CC-Expansion) on the instance segmentation map. To the best of our knowledge, this post-processing method is novel in the field of cell instance segmentation. We emphasize that we do not train on the post-processing task explicitly. An overview of this process can be seen in Figure 2.

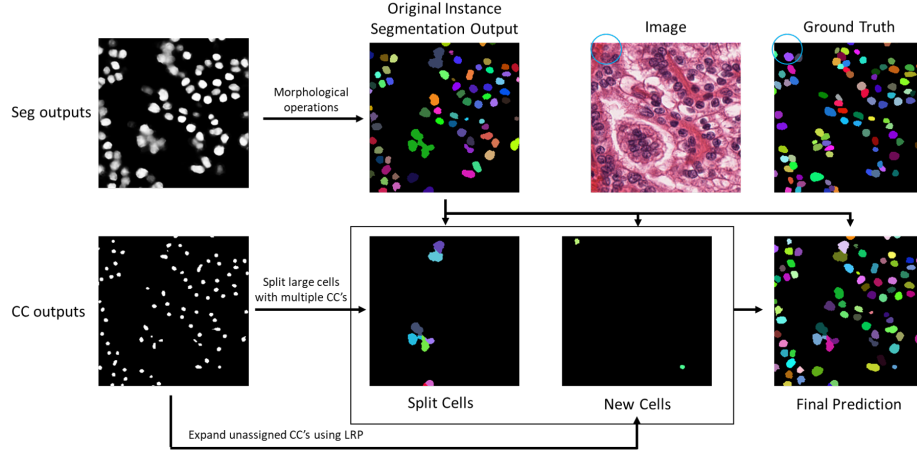


**Fig. 2.** An overview of our two-step procedure of Instance-Splitting and CC-Expansion.

The first step is the Instance-Splitting step. We first condense all blobs of CC outputs into single CC points by applying the same morphological operations

and taking the center of each blob instance. Then, we find instances in our instance segmentation map that cover two or more CC points. Intuitively, these identified instances are clumps that contain two or more cells in close proximity. We perform a simple procedure to split these clumps up, by assigning each point in the clump to its nearest CC point in L1 distance. While other distance measures and procedures can be considered, in our experiments the simple L1 distance seems to work rather well. Note that this step does not change any pixel-level metrics as it just splits existing instances. This step works well to improve object metrics when cells are more likely to be in clumps.

In the CC-Expansion step, we expand CC predictions that are not contained in any instances in our original segmentation map. Intuitively, these represent CC points of cells that should have been identified but were somehow missed in the segmentation map. Using a single backward pass in LRP on the identified blobs in the CC outputs, we obtain an "explanation" heatmap of the positive cell-center predictions, which closely resembles the shape of those cells. After applying a heatmap threshold, an approximate instance segmentation of the cells in the original image is obtained. In order to prevent repeat cells or generating new clumps of cells, an overlap threshold is implemented to discard instances with large overlaps with any existing cells. This situation happens occasionally on some oddly-shaped cells or clumps of cells.

As the difference in cell sizes can be very large, we find that the overlap threshold ( $\frac{|Cell_1 \cap Cell_2|}{\min(|Cell_1|, |Cell_2|)}$ ) works better than the IoU threshold which is more commonly used. In practice, we find that the cells found by this step are often small, obscure and sometimes even unlabelled in the ground truth annotations. We discuss this further in the results section.

## 4 Experiment details

For the baseline model, we used the same U-Net architecture as [7], and used their pre-trained weights throughout our experiments. Notably, this U-Net does not use a ResNet encoder unlike [21,27], and we get a similar level of accuracy. For the CC output branch, two additional 3x3 Conv-BatchNorm-Relu layers are added for better performance.

Each model was trained for 200 epochs using an Adam optimizer with a learning rate of 0.001. For all configurations,  $\alpha_V = 50$ ,  $\alpha_C = 50$ . We set  $\alpha_P = 200$  when we do not use  $L_{FRW}$ , otherwise  $\alpha_P = 100$ ,  $\alpha_{FRW} = 100$ . Additionally, the threshold for small objects is set to be 5. The data was augmented using random resizing, rotations, flips, crops and affine transformations.

At the testing phase, we set our CC confidence threshold to be 0.1, heatmap threshold to be 0.05 and overlap threshold to be 0.5. We found these values to work in general and they did not require much tuning. In principle, we can tune these values using our best model on the validation set before testing, but we would like to keep our procedure simple.

We evaluated our methods on the MoNuSeg (Multi-Organ Nucleus Segmentation) dataset [16] and the TNBC (Triple Negative Breast Cancer) dataset

[18]. These datasets are publicly available. MoNuSeg contains 30 fully-annotated 1000x1000 H&E stained histology images of different organs. TNBC contains 50 fully-annotated 512x512 H&E stained histology images from different parts of tissue of patients with the same cancer type. Following the procedure of [30,27], we perform 10-fold cross-validation on both of them, taking the ratio of training:validation:test to be 8:1:1. As computing the object-level metrics is computationally intensive, during cross-validation we compute pixel-level metrics once every 10 epochs and select the model with the best pixel-level F1 score.

## 5 Results and Discussion

We report our experiment results on the MoNuSeg in Table 1 and TNBC in Table 2. We report 4 scores: Pixel-wise accuracy, Pixel-wise F1 score, Object-level DICE and AJI. Object-level DICE is a weighted sum of pixel-wise F1 scores between each ground truth cell and the best assigned segmented object, as well as between each segmented object and the best assigned ground truth, with the weights being the size of the ground truth/segmented object. AJI is a Jaccard overlap between the set of ground truths and segmented objects, but only taking pairwise union and intersection between each ground truth and its assigned "best" proposal. Both AJI and Object-level DICE are object-level metrics that are important to making our case and can take values between 0 and 1. More information about Object-level DICE and AJI can be found in [21].

The segmentation baseline is the baseline method taken from [21]. We evaluate the scenarios where we only apply the Instance-Splitting procedure (Split), and where we apply both the Instance-Splitting and CC-Expansion procedures (Split + Expand). We also evaluate the effectiveness of the FRW loss by applying it on different layers of our U-Net (enc1, enc3, bottleneck). The layer that we use for the FRW loss is indicated in brackets.

**Table 1.** Results on MoNuSeg dataset. The best results have been indicated in bold.

Configuration	Acc	Pixel F1	DICE	AJI
Seg (baseline)	0.8816	0.7494	0.7044	0.4900
Seg + Split	0.8816	0.7494	0.7170	0.5262
Seg + Split + Expand	0.8815	0.7493	0.7165	0.5260
Seg (FRW bottleneck) + Split	0.8796	0.7436	0.7156	0.5269
Seg (FRW bottleneck) + Split + Expand	0.8792	0.7434	0.7148	0.5267
Seg (FRW enc3) + Split	0.8813	0.7460	0.7213	0.5327
Seg (FRW enc3) + Split + Expand	0.8810	0.7456	0.7206	0.5324
Seg (FRW enc1) + Split	0.8816	0.7497	<b>0.7220</b>	<b>0.5352</b>
Seg (FRW enc1) + Split + Expand	0.8814	0.7494	0.7214	0.5349

Firstly, we observe that the Instance Splitting step gives a substantial improvement in object-level metrics of DICE and AJI in all settings. This is supplemented by our qualitative observations of the images. An example can be

**Table 2.** Results on TNBC dataset. The best results have been indicated in bold.

Configuration	Acc	Pixel F1	DICE	AJI
Seg (baseline)	0.9355	0.7207	0.7065	0.5209
Seg + Split	0.9355	0.7207	0.7083	0.5282
Seg + Split + Expand	0.9351	0.7191	0.7065	0.5265
Seg (FRW bottleneck) + Split	0.9368	0.7249	<b>0.7147</b>	0.5393
Seg (FRW bottleneck) + Split + Expand	0.9365	0.7242	0.7137	<b>0.5394</b>
Seg (FRW enc3) + Split	0.9378	0.7312	0.7138	0.5316
Seg (FRW enc3) + Split + Expand	0.9376	0.7309	0.7133	0.5316
Seg (FRW enc1) + Split	0.9372	0.7239	0.7099	0.5337
Seg (FRW enc1) + Split + Expand	0.9365	0.7218	0.7074	0.5318

seen in Figure 2, where several larger instances were split well. A larger example can be seen in the supplementary material. It is worthwhile to note that such substantial gains, particularly on the MoNuSeg dataset, are brought by a simple CC-prediction and L1-partitioning procedure at prediction time. The CC output head was not explicitly trained for this task. Although there is little basis for comparison, we carefully note that the DICE metric of our much-simpler method is slightly better than the fully weakly-supervised version in [29] on MoNuSeg.

Next, we observe that the CC-Expansion method does not seem to improve the object-level metrics much. We find two reasons for this. Firstly, not many instances are generated in this step, and the cells produced by this method are very small, which leads to minimal impact on DICE or AJI as those metrics are weighted based on the size of the instances. Secondly, upon a visual inspection, we find that many of the small cells detected by this method are not annotated properly. An example is circled in blue in Figure 2 and more examples can be seen in the supplementary material. Usage of the CC-Expansion method seems more situational, and will be useful when there are small and obscure cells.

Lastly, we observe that the FRW loss does provide consistent improvements in our object-level metrics on both datasets. Interestingly, for MoNuSeg the most improvement came when we applied it on our "enc1" layer, which is the first layer, while for TNBC we observed the most improvement when the FRW loss was applied to the "bottleneck" layer. Curiously, our results also suggest that the loss should be applied onto the earlier layers for MoNuSeg (performance improves from bottleneck to enc3 to enc1) while it is the opposite for TNBC.

## 6 Conclusion

This paper proposes a novel and simple two-step prediction-time method (*Split* and *Expand*) for weakly supervised cell instance segmentation. We train our model to also output CC predictions but no further explicit training is needed. We test the method on MoNuSeg and TNBC datasets, observing both quantitative and qualitative improvements. Addition of the FRW loss is also shown to be effective in CC detection.



## References

1. Anders, C.J., Marinč, T., Neumann, D., Samek, W., Müller, K.R., Lapuschkin, S.: Analyzing imagenet with spectral relevance analysis: Towards imagenet un-hans’ ed. arXiv preprint arXiv:1912.11425 (2019)
2. Arras, L., Montavon, G., Müller, K.R., Samek, W.: Explaining recurrent neural network predictions in sentiment analysis. In: Proceedings of the 8th Workshop on Computational Approaches to Subjectivity, Sentiment and Social Media Analysis. pp. 159–168 (2017)
3. Arras, L., Osman, A., Müller, K.R., Samek, W.: Evaluating Recurrent Neural Network Explanations. In: Proceedings of the ACL 2019 BlackboxNLP Workshop on Analyzing and Interpreting Neural Networks for NLP. pp. 113–126. ACL (2019)
4. Bach, S., Binder, A., Montavon, G., Klauschen, F., Müller, K.R., Samek, W.: On pixel-wise explanations for non-linear classifier decisions by layer-wise relevance propagation. PLOS ONE **10**(7), e0130140 (2015)
5. Beck, A.H., Sangoi, A.R., Leung, S., Marinelli, R.J., Nielsen, T.O., van de Vijver, M., West, R.B., van de Rijn, M., Koller, D.: Systematic analysis of breast cancer morphology uncovers stromal features associated with survival. Science Translational Medicine **3**, 108ra113 – 108ra113 (2011)
6. Boutros, M., Heigwer, F., Laufer, C.: Microscopy-based high-content screening. Cell **163**(6), 1314 – 1325 (2015)
7. Buda, M., Saha, A., Mazurowski, M.A.: Association of genomic subtypes of lower-grade gliomas with shape features automatically extracted by a deep learning algorithm. Computers in Biology and Medicine **109**, 218 – 225 (2019)
8. Chamanzar, A., Nie, Y.: Weakly supervised multi-task learning for cell detection and segmentation. In: 2020 IEEE 17th ISBI. pp. 513–516. IEEE (2020)
9. Chen, L., Strauch, M., Merhof, D.: Instance segmentation of biomedical images with an object-aware embedding learned with local constraints. In: MICCAI. pp. 451–459. Springer (2019)
10. Filipczuk, P., Fevens, T., Krzyżak, A., Monczak, R.: Computer-aided breast cancer diagnosis based on the analysis of cytological images of fine needle biopsies. IEEE T-MI **32**(12), 2169–2178 (2013)
11. Graham, S., Vu, Q.D., Raza, S.E.A., Azam, A., Tsang, Y.W., Kwak, J.T., Rajpoot, N.: Hover-net: Simultaneous segmentation and classification of nuclei in multi-tissue histology images. Medical Image Analysis **58**, 101563 (2019)
12. Halliwell, N., Lecue, F.: Trustworthy convolutional neural networks: A gradient penalized-based approach. arXiv preprint arXiv:2009.14260 (2020)
13. Hesamian, M.H., Jia, W., He, X., Kennedy, P.: Deep learning techniques for medical image segmentation: Achievements and challenges. Journal of digital imaging **32**(4), 582–596 (August 2019)
14. Kauffmann, J., Esders, M., Montavon, G., Samek, W., Müller, K.R.: From clustering to cluster explanations via neural networks. arXiv:1906.07633 (2019)
15. Kohlbrenner, M., Bauer, A., Nakajima, S., Binder, A., Samek, W., Lapuschkin, S.: Towards best practice in explaining neural network decisions with LRP. In: IJCNN. pp. 1–7 (2020)
16. Kumar, N., Verma, R., Sharma, S., Bhargava, S., Vahadane, A., Sethi, A.: A dataset and a technique for generalized nuclear segmentation for computational pathology. IEEE T-MI **36**(7), 1550–1560 (2017)
17. Lapuschkin, S., Wäldchen, S., Binder, A., Montavon, G., Samek, W., Müller, K.R.: Unmasking clever hans predictors and assessing what machines really learn. Nature Communications **10**(1), 1096 (2019)

18. Naylor, P., Laé, M., Reyat, F., Walter, T.: Segmentation of nuclei in histopathology images by deep regression of the distance map. *IEEE T-MI* **38**(2), 448–459 (2019)
19. Obikane, S., Aoki, Y.: Weakly supervised domain adaptation with point supervision in histopathological image segmentation. In: Cree, M., Huang, F., Yuan, J., Yan, W.Q. (eds.) *Pattern Recognition*. pp. 127–140. Springer Singapore, Singapore (2020)
20. Poerner, N., Roth, B., Schütze, H.: Evaluating neural network explanation methods using hybrid documents and morphosyntactic agreement. In: *Proceedings of the 56th ACL (Volume 1: Long Papers)*. p. 340–350. ACL (2018)
21. Qu, H., Wu, P., Huang, Q., Yi, J., Riedlinger, G.M., De, S., Metaxas, D.N.: Weakly supervised deep nuclei segmentation using points annotation in histopathology images. In: *International Conference on Medical Imaging with Deep Learning*. pp. 390–400 (2019)
22. Qu, H., Wu, P., Huang, Q., Yi, J., Yan, Z., Li, K., Riedlinger, G.M., De, S., Zhang, S., Metaxas, D.N.: Weakly supervised deep nuclei segmentation using partial points annotation in histopathology images. *IEEE T-MI* **39**(11), 3655–3666 (Nov 2020)
23. Samek, W., Binder, A., Montavon, G., Lapuschkin, S., Müller, K.R.: Evaluating the visualization of what a deep neural network has learned. *IEEE TNNLS* **28**(11), 2660–2673 (2016)
24. Schnake, T., Eberle, O., Lederer, J., Nakajima, S., Schütt, K.T., Müller, K.R., Montavon, G.: XAI for Graphs: Explaining graph neural network predictions by identifying relevant walks. *arXiv preprint arXiv:2006.03589* (2020)
25. Sun, J., Lapuschkin, S., Samek, W., Binder, A.: Understanding image captioning models beyond visualizing attention. *arXiv preprint arXiv:2001.01037* (2020)
26. Sun, J., Lapuschkin, S., Samek, W., Zhao, Y., Cheung, N.M., Binder, A.: Explanation-guided training for cross-domain few-shot classification. *arXiv preprint arXiv:2007.08790* (2020)
27. Tian, K., Zhang, J., Shen, H., Yan, K., Dong, P., Yao, J., Che, S., Luo, P., Han, X.: Weakly-supervised nucleus segmentation based on point annotations: A coarse-to-fine self-stimulated learning strategy. In: Martel, A.L., Abolmaesumi, P., Stoyanov, D., Mateus, D., Zuluaga, M.A., Zhou, S.K., Racocanu, D., Joskowicz, L. (eds.) *MICCAI 2020*. pp. 299–308. Springer International Publishing, Cham (2020)
28. Ulman, V., Maška, M., Magnusson, K., Ronneberger, O., Haubold, C., Harder, N., Matula, P., Matula, P., Svoboda, D., Radojevic, M., Smal, I., Rohr, K., Jaldén, J., Blau, H., Dzyubachyk, O., Lelieveldt, B., Xiao, P., Li, Y., Cho, S.Y., Ortiz-de Solorzano, C.: An objective comparison of cell tracking algorithms. *Nature Methods* **14** (12 2017)
29. Yen, T.A., Hsu, H.C., Pati, P., Gabrani, M., Foncubierta-Rodríguez, A., Chung, P.C.: Ninepins: Nuclei instance segmentation with point annotations. *arXiv preprint arXiv:2006.13556* (2020)
30. Yoo, I., Yoo, D., Paeng, K.: Pseudoedgenet: Nuclei segmentation only with point annotations. In: *MICCAI*. pp. 731–739. Springer (2019)